AD-A064 132 TETRA TECH INC PASADENA CALIF F/G 20/4
NONLINEAR THEORY FOR PARTIALLY CAVITATING CASCADE FLOWS.(U)
SEP 78 O FURUYA N00014-78-C-0146
UNCLASSIFIED TETRAT-TC-3951-01 NL

| OF |
AD
A064132

END
DATE
FILMED
4-79
DDC

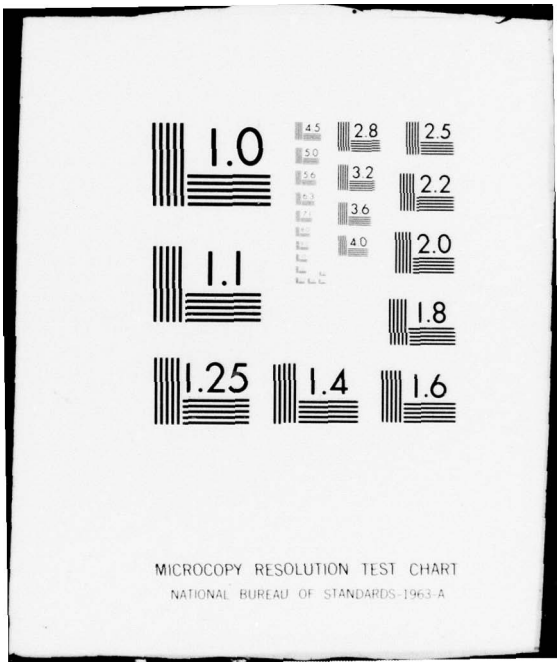
1.0
1.1
1.25
1.4
1.6
1.8
2.0
2.2
2.5
2.8
3.2
3.6
4.0
4.5
5.0
5.6
6.3
MICROCOPY RESOLUTION TEST CHART
NATIONAL BUREAU OF STANDARDS-1963-A

Report No. TC 3951-01
Contract No. N00014-78-C-0146

NONLINEAR THEORY FOR PARTIALLY CAVITATING CASCADE FLOWS

By

OKITSUGU FURUYA

TETRA TECH, INC.
630 NORTH ROSEMEAD BOULEVARD
PASADENA, CALIFORNIA 91107

SEPTEMBER, 1978

Prepared for
DAVID W. TAYLOR NAVAL SHIP R&D CENTER
BETHESDA, MARYLAND 20084

OFFICE OF NAVAL RESEARCH
800 NORTH QUINCY STREET
ARLINGTON, VIRGINIA 22217

Report No. TC 3951-01
Contract No. N00014-78-C-0146

NONLINEAR THEORY FOR PARTIALLY CAVITATING CASCADE FLOWS

By

OKITSUGU FURUYA

TETRA TECH, INC.
630 NORTH ROSEMEAD BOULEVARD
PASADENA, CALIFORNIA 91107

SEPTEMBER, 1978

Prepared for
DAVID W. TAYLOR NAVAL SHIP R&D CENTER
BETHESDA, MARYLAND 20084

OFFICE OF NAVAL RESEARCH
800 NORTH QUINCY STREET
ARLINGTON, VIRGINIA 22217

Approved for public release;
distribution unlimited

SECURITY CLASSIFICATION OF THIS PAGE (When Data Entered)

REPORT DOCUMENTATION PAGE

READ INSTRUCTIONS BEFORE COMPLETING FORM

1. REPORT NUMBER: TC 3951-01

2. GOVT ACCESSION NO.:

3. RECIPIENT'S CATALOG NUMBER:

4. TITLE (and Subtitle): (6) Nonlinear Theory for Partially Cavitating Cascade Flows.

5. TYPE OF REPORT & PERIOD COVERED: Technical-Theory, February 15, 1978-Oct. 15, 1978

6. PERFORMING ORG. REPORT NUMBER: TC 3951-01

7. AUTHOR(s): (10) Okitsugu Furuya

8. CONTRACT OR GRANT NUMBER(s): (15) N00014-78-C-0146

9. PERFORMING ORGANIZATION NAME AND ADDRESS:
TETRA TECH, INC.
630 North Rosemead Boulevard
Pasadena, California 91107

10. PROGRAM ELEMENT, PROJECT, TASK AREA & WORK UNIT NUMBERS:
DWTNSR&DC
824196/79-1-77(1505)

11. CONTROLLING OFFICE NAME AND ADDRESS:
David W. Taylor Naval Ship R&D Center
Department of the Navy
Bethesda, Maryland 20084

12. REPORT DATE: (11) September 1978

13. NUMBER OF PAGES: 37

14. MONITORING AGENCY NAME & ADDRESS (if different from Controlling Office):
Office of Naval Research
800 North Quincy Street
Arlington, Virginia 22217
(12) 47 p.

15. SECURITY CLASS. (of this report): Unclassified

15a. DECLASSIFICATION/DOWNGRADING SCHEDULE:

16. DISTRIBUTION STATEMENT (of this Report):

Approved for public release; distribution unlimited

(14) TETRA-TC-3951-01

17. DISTRIBUTION STATEMENT (of the abstract entered in Block 20, if different from Report):

(9) Technical rept. 15 Feb – 15 Oct 78,

18. SUPPLEMENTARY NOTES

Sponsored by the Naval Sea Systems Command General Hydrodynamic Research Program and administered by the David W. Taylor Naval Ship R&D Center, Code 1505, Bethesda, Maryland 20084.

19. KEY WORDS (Continue on reverse side if necessary and identify by block number)

Partial cavity flow
Cascade
Nonlinear theory

20. ABSTRACT (Continue on reverse side if necessary and identify by block number)

A nonlinear theory for solving partially cavitating cascade problems was formulated in two different types of input data set-ups, one specifying cavitation number and the other the cavity length. The second method was necessary to find a unique solution because the cavity length has two different values for a specified cavitation number in some blade geometry cases. This fact, together with the investigation of detailed pressure distributions on the upper wetted part of the blade, explained the unsteady cavity phenomena previously reported in some experiments. Suggestions were made on how to avoid the occurrence of the unsteady partial cavity phenomena when one designs fluid machinery used in a partially cavitating regime.

DD FORM 1 JAN 73 1473 EDITION OF 1 NOV 65 IS OBSOLETE
S/N 0102-014-6601

403 146

SECURITY CLASSIFICATION OF THIS PAGE (When Data Entered)

TABLE OF CONTENTS

I. SUMMARY

A nonlinear theory for solving partially cavitating cascade problems was formulated in two different types of input data set-ups, one specifying cavitation number and the other the cavity length. The second method was necessary to find a unique solution because the cavity length has two different values for a specified cavitation number in some blade geometry cases. This fact, together with the investigation of detailed pressure distributions on the upper wetted part of the blade, explained the unsteady cavity phenomena previously reported in some experiments. Suggestions were made on how to avoid the occurrence of the unsteady partial cavity phenomena when one designs fluid machinery used in a partially cavitating regime.

II. ACKNOWLEDGMENTS

This research was carried out under the Naval Sea Systems Command, General Hydromechanics Research Program, administered by the David Taylor Naval Ship Research and Development Center, Contract N00014-78-C-0146. The author is indebted to Mr. Peter Roshko for conducting numerical computations throughout the project.

III. LIST OF FIGURES

IV. NOMENCLATURE

$\tilde{A}$	scale factor for mapping between W and ζ planes.
b	ξ-coordinate corresponding to the upper cavity separation point
c	ξ-coordinate corresponding to the cavity reattachment position and also used as a chord length of blade
C_L, C_D	lift and drag coefficients parallel and normal to the incoming flow direction $\left(= L \text{ or } D/\tfrac{1}{2}\ \rho U_1^2\ c\right)$
$\bar{C}_L, \bar{C}_D$	lift and drag coefficients in the direction of the x and y axes
C_{Lm}	lift coefficients in the x-direction normalized by the geometric mean velocity U_m
C_p	pressure coefficient $\left(= \left(p-p_1\right)/\tfrac{1}{2}\ \rho U_1^2\right)$
D	drag force
d	spacing of cascade blades
f	ξ-coordinate corresponding to the upper trailing edge
f_i	nonlinear equations representing the boundary value problem for unknown solution parameters x_i
i	index for complex variable $\left(= \sqrt{-1}\right)$
L	lifting force
ℓ_c	cavity length
p	static pressure
q	flow velocity modulus
S_1, S_2	total arc lengths of the upper and lower wetted part of the blade, respectively

$s(\xi)$	local arc length measured from either the leading edge or the reattachment point of cavity
$sg(x)$	sign function $\begin{cases} = 1 \text{ for } x \geq 0 \\ = -1 \text{ for } x < 0 \end{cases}$
TH	thickness of plano-convex blade normalized by chord
U	flow velocity amplitude
W	complex potential $= (\Phi + i\Psi)$
z	physical plane $(= x+iy)$
α	flow angle made with the x-axis of the physical plane
β	local blade slope measured from the x-axis, clockwise negative; for the second arc S_2, $-\pi$ is to be added
γ	geometric stagger angle
δ	stagger angle of the potential plane cascade set-up $(= \alpha_1 + \gamma)$
ζ	transform potential plan $(= \xi + i\eta)$
ζ_1	ζ-coordinate corresponding to the upstream infinity of the physical plane
η	vertical coordinate in the ξ-plane
θ	flow angle
ξ	horizontal coordinate in the ζ-plane
σ	cavitation number $(= (p_1 - p_c)/\frac{1}{2}\rho U_1^2)$
τ	logarithmic velocity normalized by U_2 $(= \ell n(q/U_2))$
Φ	potential function
Ψ	stream function
ω	hodograph variable $(= \theta + i\tau)$

Subscripts:

1 and 2	denotes quantities belonging to the upstream and downstream infinities, respectively, or quantities belonging to the first and second arcs, respectively
c	denotes the cavity
m	denotes geometric mean quantities

Superscripts:

+, -,	quantities belonging to the immediate upper and lower sides of the ξ-axis

1. INTRODUCTION

It is a common practice that hydrodynamists avoid high speed fluid machinery or components to be used under partially cavitating conditions because many adverse hydrodynamic effects exist for such conditions. One of the most important phenomena is that of cavitation damage caused by cavity bubble collapse taking place near the material. This material damage is so severe that components such as marine propellers after several hundred hours of exposure to cavity collapse will become totally out of use (see e.g. [1]* for such examples). Furthermore, it was found in experiments that partially cavitating flows experience inherent unsteady flow phenomena; the length of cavity changes from a very short one to one chord length in an oscillatory way (see e.g. [2] and [3]). It is for this reason that effort by the designer is directed toward either totally avoiding cavitating conditions, if this is possible, or purposely generating <u>supercavitating</u> conditions in which cavity length is larger than the body and thus bubble collapse occurs behind the material.

However, in recent years some marine and fluid machinery have quite often been used in the partially cavitating flow regime. One such example is in the marine propeller area; convential and supercavitating propellers are sometimes used under off-design conditions, the former at a lower advance speed and the latter

---

* Numbers in brackets designate references at end of paper.

at a higher advance speed than that of the design point. In both cases some portions of propeller blades have partial cavities as were shown in experimental works by Sontvedt [4], Bohn [5] and Peck [6].

There exists more positive designers' attitude of using the partially cavitating condition in some area of fluid machinery such as pump inducers. Cavitating inducers used, for example, in liquid propellant rockets always operate at a partially cavitating condition. Because of simplicity, such inducer blades are made of helical profile having long straight-line face. The cavity length is designed to be always shorter than the chord length (see the work of Acosta [7]).

Interest has therefore grown recently in how to analytically determine the force coefficients of partially cavitating single foil or cascade blades. Linearized theories were applied by many researchers for both single and cascade blades. The former include works by Acosta [8], Geurst [9], Geurst and Verbrugh [10], Wade [11] and Golden [12]. Acosta [8] and Geurst [9] treated the flat plate single foil problem and Geurst and Verbrugh [10] solved the problem for camber line profiles. Wade [11] and Golden [12] considered both camber and thickness effects in the same linearized theory framework but with different solution methods; the former used an analytical solution method for vortex and source distributions whereas the latter employed a

numerical method to determine the strength of the singularities. For cascade configurations, Wade [13] solved flat plate cascade problems in exactly the same manner as for single foils. Algebra for the cascade flow becomes more complicated due to extra cascade mapping necessary for this case.

As has been seen above, all the existing analytical methods regarding the partially cavitating flow employed the linearized theories. The limitations of such theories are well described in each paper [8-13]; any perturbed flow quantities due to the existence of cavity and obstacle in the uniform flow should be small. Ranges of flow incidence angle, cavitation number and camber of blades for which the accuracy of the linearized theory is maintained to a desirable degree are not known until comparisons with experiments are made. Questions particularly arise for the linearization procedure for the nonlinear boundary condition on the cavity wall. Unlike the supercavitating flow regime, the cavitation number σ is relatively large compared to the uniform flow velocity. Nevertheless, all the linearized theories mentioned above assumed σ to be small. Furthermore, partially cavitating flow around the cascade having relatively high solidity will generate large disturbed velocity components for which the application of the linearized theory is no longer valid.

Under the circumstances just described, an analytical tool for determining the hydrodynamic forces of partially cavitating

cascade blades has been developed. The method used here is the nonlinear potential theory, covering a complete range of geometric configurations and flow parameters without generating any inaccuracies in satisfying the boundary conditions. The method is quite similar to that used for supercavitating cascade flow analysis by Furuya [14], but with substantial increase in complexity both in mathematical formulation and numerical computations.

In the following sections, mathematical formulations and numerical methods will be described. Some representative numerical results will be compared with those of a linearized theory [13] and an experiment [3].

2. NONLINEAR BOUNDARY VALUE PROBLEM

A mathematical model representing the physical flow of partial cavity around the cascade has to be established prior to the formulation of a nonlinear boundary value problem. The reattachment of cavity on the upper portion of the blade makes such a flow model construction difficult. Highly turbulent flows near the end point of cavity cannot be accurately represented within the framework of potential flow assumption currently taken. Among many possible flow models, we have chosen a most realistic one as shown in Figure 1. The cavity streamline detached from the leading edge of the blade terminates at point C, the location of which is either specified or determined as part of the solution as a function of cavitation number. This depends upon the type of input for boundary conditions, i.e., whether ℓ_c or σ is used as input data. Then the same streamline follows the body profile $\beta_2(x)$ through the trailing edge. The gap existing between the streamline and the upper body boundary is considered to be a turbulent wake region, which is implicitly eliminated from the present potential theory analysis. From the trailing edge, the wake with a constant pressure condition extends to the downstream infinity and is assumed to close there.

The end point of cavity is interesting from both physical and mathematical viewpoints. In the present flow model, the point C is termed as a single spiral vortex model named after Tulin

[16]. From the cavity side the streamline curls in to a point C, then immediately follows the corresponding body slope. It seems that this behavior of the streamline more or less represents the cavity collapse in the actual flow situation.

It must be noted that this type of cavity closure model may not be suitable for very thick foil cases, since the gap between the streamline and body boundary mentioned above is out of control. It may happen that the cavity ends inside the blade structure if the blade thickness is large. For such cases, one has to use an open wake cavity model in which the cavity closure condition at down infinity is relaxed but instead replaced by specifying the cavity thickness at the end point of cavity. In this way the streamline crossing problem mentioned above will be totally eliminated. The mathematical formulation for the open wake model is no more complicated than the closed wake. In this paper, however, the latter will be used throughout investigation.

The mathematical formulation is quite similar to that of the supercavitating cascade flow problem in [14], thus repetition of detailed explanations will be avoided.

The partially cavitating flow around the cascade shown in Figure 1 is first mapped onto the potential plane $W = \Phi+i\Psi$ and then to the upper half of the transform plane ζ by the cascade mapping function, see Figures 2(a) and (b), respectively. The

cascade mapping function and its derivative are given by the following equations:

$$W = \frac{d}{2\pi}\left\{e^{-i\delta}\ln(1-\zeta/\zeta_1) + e^{i\delta}\ln(1-\zeta/\bar{\zeta}_1)\right\} \tag{1}$$

where

$$\zeta_1 = \tilde{A}\, e^{i(\pi/2-\delta)} \tag{2}$$

$$\delta = \alpha_1+\gamma, \tag{3}$$

and $\tilde{A}$ is a scaling factor between the two planes, yet to be known. Thus, the derivative of W on the ξ axis is given

$$\frac{dW}{d\xi} = \frac{d}{\pi}\,\frac{\xi\cos\delta}{(\xi-\tilde{A}\sin\delta)^2 + (\tilde{A}\cos\delta)^2}. \tag{4}$$

The stagger angle δ of the W-plane cascade set-up in Equation (3) was determined by the coordinate point (Φ_0, Ψ_0) where

$$\begin{aligned}\Phi_0 &= dU_1\cdot\sin(\alpha_1+\gamma)\\ \Psi_0 &= dU_1\cdot\cos(\alpha_1+\gamma).\end{aligned} \tag{5}$$

Introducing a hodograph variable ω

$$\frac{dW}{dz} = q\, e^{-i\theta} = U_2 e^{-i\omega} \tag{6}$$

or

$$\omega = \theta+i\,\tau \tag{7}$$

$$\tau = \ln(q/U_2) \tag{8}$$

where U_2 denotes the velocity at downstream infinity, we can express the boundary conditions on the real axis ξ in the ζ-plane as follows:

(i) $\tau = 0 \quad , \quad -\infty < \xi < -1 \quad , \quad f < \xi < \infty$

(ii) $\tau = \ell n \ (\sqrt{1 + \sigma}/U_2) \quad , \quad b < \xi < c$

(iii) $$\theta = \begin{cases} \beta_1 \ (\equiv \tan^{-1} dy/dx) & -1 < \xi < 0 \\ \beta_1 + \pi & 0 < \xi < b \\ \beta_2 + \pi & c < \xi < f. \end{cases}$$

This is a typical mixed-type boundary value problem, the solution of which can readily be found by the same approach as used in [14], but in a somewhat more complicated form due to the existence of two branch cuts, $-1 < \xi < b$ and $c < \xi < f$.

Analytically continuing the upper half of ξ-plane into the lower half plane with $\omega(\xi^*) = \omega^*(\xi)$, where * denotes the complex conjugate, these boundary conditions (i) - (iii) will be expressed as follows:

(i) $\omega^+ - \omega^- = 0 \ ; \ -\infty < \xi < -1, \quad f < \xi < \infty$

(ii) $\omega^+ - \omega^- = 2i\ell n\left(\sqrt{1+\sigma}/U_2\right); \quad b < \xi < c$

(iii) $$\omega^+ + \omega^- = \begin{cases} 2\beta_1 & ; \ -1 < \xi < 0 \\ 2(\beta_1 + \pi); & 0 < \xi < b \\ 2(\beta_2 + \pi); & c < \xi < f. \end{cases}$$

The homogeneous part of the solution $H(\xi)$ for which the right hand sides of (i) - (iii) are all zero is obtained by considering the singularity at the end point of cavity and no singularities anywhere else;

$$H(\zeta) = \sqrt{\frac{(\zeta+1)(\zeta-b)(\zeta-f)}{\zeta-c}} \quad . \tag{9}$$

The general solution $G(\zeta)$ satisfying the mixed boundary conditions is defined by $G(\zeta) = \omega(\zeta)/H(\zeta)$ and obtained by applying the Cauchy integral formula;

$$G(\zeta) = \frac{1}{2\pi i} \int (G^+ - G^-) \frac{d\xi'}{\xi' - \zeta} .$$

Therefore,

$$\omega(\zeta) = H(\zeta)G(\zeta)$$

$$= \sqrt{\frac{(\zeta+1)(\zeta-b)(\zeta-f)}{\zeta-c}} \frac{1}{2\pi i} \left\{ \int_{-1}^{b} \frac{2\beta_1}{i\sqrt{\frac{(\xi'+1)(b-\xi')(\xi'-f)}{\xi'-c}}} \frac{d\xi'}{\xi'-\zeta} \right.$$

$$+ \int_{0}^{b} \frac{2\pi}{i\sqrt{\frac{(\xi'+1)(b-\xi')(\xi'-f)}{\xi'-c}}} \frac{d\xi'}{\xi'-\zeta} + \int_{b}^{c} \frac{2i \ \ell n\left(\sqrt{1+\sigma}/U_2\right)}{\sqrt{\frac{(\xi'+1)(\xi'-b)(\xi'-f)}{\xi'-c}}} \frac{d\xi'}{\xi'-\zeta}$$

$$\left. + \int_{c}^{f} \frac{2\beta_2+2\pi}{i\sqrt{\frac{(\xi'+1)(\xi'-b)(f-\xi')}{\xi'-c}}} \frac{d\xi'}{\xi'-\zeta} \right\} . \tag{10}$$

2.1 BOUNDARY VALUE PROBLEM TYPE I (SPECIFY CAVITATION NUMBER σ)

For the problem in which the cavitation number is specified as an input parameter, the length of cavity is to be determined as part of the solution. In such a problem we have a total of six unknown quantities, U_2, α_2, $\tilde{A}$, b, c, f, requiring six equations to determine them uniquely;

(i) At the upstream infinity, $\omega(\zeta_1) = \alpha_1 + i\ \ell n(1/U_2)$: 2 equations

(ii) At the downstream infinity, $\omega(\infty) = \alpha_2$: 1 equation

(iii) Length of First Arc $\equiv S_1$: 1 equation

(iv) End point of the streamline (ξ=f) matches the physical trailing edge: 1 equation

(v) Continuity Equation: 1 equation

where S_1 and S_2 are depicted in Figure 2(c). It is noted that the arc length condition (iv) replaces the potential difference condition in the supercavitating cascade problem. (see Reference [14])

Application of these conditions to Equation (10) yields the following six equations;

i) <u>At Upstream Infinity:</u>

$$\begin{Bmatrix} f_1 \\ f_2 \end{Bmatrix} \equiv \sqrt{\frac{(\zeta_1+1)(\zeta_1-b)(\zeta_1-f)}{\zeta_1-c}} \Bigg\{ - \frac{1}{\pi}\int_{-1}^{b} \frac{\beta_1}{\sqrt{\frac{(\xi'+1)(b-\xi')(\xi'-f)}{\xi'-c}}} \frac{d\xi'}{\xi'-\zeta_1}$$

$$- \int_{0}^{b} \frac{1}{\sqrt{\frac{(\xi'+1)(b-\xi')(\xi'-f)}{\xi'-c}}} \frac{d\xi'}{\xi'-\zeta_1} + \frac{1}{\pi}\ell n\left(\frac{\sqrt{1+\sigma}}{U_2}\right) x$$

$$\int_{b}^{c} \frac{1}{\sqrt{\frac{(\xi'+1)(\xi'-b)(\xi'-f)}{\xi'-c}}} \frac{d\xi'}{\xi'-\zeta_1} - \frac{1}{\pi}\int_{c}^{f} \frac{\beta_2+\pi}{\sqrt{\frac{(\xi'+1)(\xi'-b)(f-\xi')}{\xi'-c}}} \frac{d\xi'}{\xi'-\zeta_1} \Bigg\}$$

$$- \left\{ \alpha_1 + i\ \ell n(1/U_2) \right\} = 0 \qquad (11)$$

ii) At Downstream Infinity:

$$f_3 \equiv \frac{1}{\pi}\int_{-1}^{b} \frac{\beta_1}{\sqrt{\frac{(\xi'+1)(b-\xi')(\xi'-f)}{\xi'-c}}}\, d\xi' + \int_{0}^{b} \frac{d\xi'}{\sqrt{\frac{(\xi'+1)(b-\xi')(\xi'-f)}{\xi'-c}}}$$

$$- \frac{1}{\pi} \ln\left(\frac{\sqrt{1+\sigma}}{U_2}\right) \int_{b}^{c} \frac{d\xi'}{\sqrt{\frac{(\xi'+1)(\xi'-b)(\xi'-f)}{\xi'-c}}} +$$

$$\frac{1}{\pi}\int_{c}^{f} \frac{\beta_2+\pi}{\sqrt{\frac{(\xi'+1)(\xi'-b)(f-\xi)}{\xi'-c}}}\, d\xi' - \alpha_2 = 0 \qquad (12)$$

iii) First Arc Length = S_1:

On the wetted part of the streamline,

$$\frac{dz}{ds_1} = e^{i\beta_1}$$

thus

$$ds_1 = e^{-i\beta}\, \frac{e^{i\omega}}{U_2}\, \frac{dW}{d\xi}\, d\xi \ .$$

For $-1 < \xi < b$, $\omega(\zeta)$ can be written as follows;

$$\omega(\xi) = \begin{cases} ig_1(\xi) + \beta_1(\xi) & , \quad -1 < \xi < 0 \\ ig_1(\xi) + \beta_1(\xi) + \pi, & \quad 0 < \xi < b \end{cases}$$

where

$$g_1(\xi) = \sqrt{\frac{(\xi+1)(b-\xi)(\xi-f)}{\xi-c}} \left\{ -\frac{1}{\pi} \oint_{-1}^{b} \frac{\beta_1}{\sqrt{\frac{(\xi'+1)(b-\xi')(\xi'-f)}{\xi'-c}}} \frac{d\xi'}{\xi'-\xi} \right.$$

$$-\oint_{0}^{b} \frac{1}{\sqrt{\frac{(\xi'+1)(b-\xi')(\xi'-f)}{\xi'-c}}} \frac{d\xi'}{\xi'-\xi} + \frac{1}{\pi} \ln \left(\frac{\sqrt{1+\sigma}}{U_2} \right) x$$

$$\left. \int_{b}^{c} \frac{1}{\sqrt{\frac{(\xi'+1)(\xi'-b)(\xi'-f)}{\xi'-c}}} \frac{d\xi'}{\xi'-\xi} - \frac{1}{\pi} \int_{c}^{f} \frac{\beta_2+\pi}{\sqrt{\frac{(\xi'+1)(\xi'-b)(f-\xi')}{\xi'-c}}} \frac{d\xi'}{\xi'-\xi} \right\} . \quad (13)$$

After integrating the above equation, one finds;

$$s_1(\xi) = \int_{\xi}^{b} sg(\xi) \frac{e^{-g_1(\xi)}}{U_2} \frac{dW}{d\xi} \, d\xi$$

where

$$sg(\xi) = \begin{cases} 1 & , \quad \xi > 0 \\ -1 & , \quad \xi < 0 . \end{cases}$$

The arc length condition is therefore satisfied by the following equation;

$$f_4 \equiv S_1 - s_1(-1) = 0 \quad (14)$$

where $dW/d\xi$ is given by Equation (4).

iv) <u>End Point of the Streamline at $\xi = f$ Matching the Trailing Edge of the Blade</u>:

Similar to the above derivation, the equation f_5 is obtained as follows:

$$f_5 \equiv S_2 - s_2(f) = 0 \tag{15}$$

where

$$s_2(\xi) = \int_c^{\xi} \frac{e^{-g_2(\xi)}}{U_2} \frac{dW}{d\xi'}\, d\xi'$$

and

$$g_2(\xi) = \sqrt{\frac{(\xi+1)(\xi-b)(f-\xi)}{\xi-c}} \left\{ - \frac{1}{\pi} \int_{-1}^{b} \frac{\beta_1}{\sqrt{\frac{(\xi'+1)(b-\xi')(\xi'-f)}{\xi'-c}}} \frac{d\xi'}{\xi'-\xi} \right.$$

$$- \int_0^b \frac{1}{\sqrt{\frac{(\xi'+1)(b-\xi')(\xi'-f)}{\xi'-c}}} \frac{d\xi'}{\xi'-\xi} + \frac{1}{\pi} \ln \left(\frac{\sqrt{1+\sigma}}{U_2} \right) x$$

$$\left. \int_b^c \frac{1}{\sqrt{\frac{(\xi'+1)(\xi'-b)(\xi'-f)}{\xi'-c}}} \frac{d\xi'}{\xi'-\xi} - \frac{1}{\pi} \int_c^f \frac{\beta_2+\pi}{\sqrt{\frac{(\xi'+1)(\xi'-b)(f-\xi')}{\xi'-c}}} \frac{d\xi'}{\xi'-\xi} \right\} \tag{16}$$

In order to determine the second arc length S_2, the end point of cavity should be known. The cavity shape is expressed in terms of ξ-coordinate;

$$x - x_B = \frac{1}{\sqrt{1+\sigma}} \int_b^{\xi} \cos g_c(\xi') \frac{dW}{d\xi'}\, d\xi' \tag{17}$$

$$y - y_B = \frac{1}{\sqrt{1+\sigma}} \int_b^{\xi} \sin g_c(\xi') \frac{dW}{d\xi'}\, d\xi' \tag{18}$$

where

$$g_c(\xi)\sqrt{\frac{(\xi+1)\ (\xi-b)\ (f-\xi)}{c-\xi}}\left\{-\frac{1}{\pi}\int_{-1}^{b}\frac{\beta_1(\xi')}{\sqrt{\frac{(\xi'+1)(b-\xi')(\xi'-f)}{\xi'-c}}}\frac{d\xi'}{\xi'-\xi}\right.$$

$$-\int_{o}^{b}\frac{1}{\sqrt{\frac{(\xi'+1)(b-\xi')(\xi'-f)}{\xi'-c}}}\frac{d\xi'}{\xi'-\xi}+\frac{1}{\pi}\ln\left(\frac{\sqrt{1+\sigma}}{U_2}\right)X$$

$$\left.\int_{b}^{c}\frac{1}{\sqrt{\frac{(\xi'+1)(\xi'-b)(\xi'-f)}{\xi'-c}}}\frac{d\xi'}{\xi'-\xi}-\frac{1}{\pi}\int_{c}^{f}\frac{\beta_2+\pi}{\sqrt{\frac{(\xi'+1)(\xi'-b)(f-\xi')}{\xi'-c}}}\frac{d\xi'}{\xi'-\xi}\right\}. \quad (19)$$

x_B, y_B are the physical coordinates of the blade leading edge. The end point of the cavity (x_c, y_c) is obtained by setting the upper bound of the above integrals (17) and (18) to be c. Once (x_c, y_c) are determined, the second arc length S_2 is easily calculated by following the body profile.

v) Continuity Equation:

The mass flow condition for the upstream and downstream is given as;

$$f_6 \equiv U_1 \cos(\alpha_1+\gamma)\cdot d - U_2 \cos(\alpha_2+\gamma)\cdot d = 0 \quad (20)$$

Equations (11), (12), (14), (15) and (20) now provide six independent relationships for six unknown parameters.

2.2 BOUNDARY VALUE PROBLEM TYPE II (SPECIFY CAVITY LENGTH ℓ_c)

The cavity length ℓ_c is used as input data in this case and the corresponding cavitation number σ is determined as a result of the solution. Minor changes to the TYPE I problem are necessary. In addition to f_5 in Equation (15), one more equation, f_7, is added in order to satisfy the fixed cavity length condition.

$$f_7 \equiv x_c - \ell_c = 0 \tag{21}$$

where x_c is calculated by setting ξ to be c in Equation (17). We have now seven independent equations for seven unknown solution parameters including σ.

There is absolutely no difference in final solutions between the above two boundary value problems as long as the physical and geometric flow conditions are the same. In many actual cases, the cavitation number, which can be simply determined by the upstream static pressure and vapor pressure, is a specified input rather than the cavity length. Only the first type of B.V.P. is therefore usually used to provide solutions for the problem like supercavitating flows. Special reasons for introducing the second type of B.V.P. in this study exist:

i) Increase the stability of the numerical iterative method by fixing the wetted portion of the upper blade, and

ii) Avoid the numerical instability caused by the existence of multiple cavity-length solutions for one cavitation number as reported in [9], [13] and [15].

As will be discussed in the following section, the numerical instability actually occurred for certain cases when the first type of B.V.P. was used, whereas cavitation number was uniquely determined for any specified cavity length when the second method was employed.

3. NUMERICAL METHOD

The same Newton's functional iterative method as that in [14] was applied to the present system of nonlinear functional equations for determining the solution parameters. Representing these equations and unknown parameters as

$$\underline{f}\ (\underline{x}) = 0, \tag{22}$$

the iterative method is introduced in the following relation;

$$J\left(\underline{x}^{(n)}\right) \cdot \left(\underline{x}^{(n+1)} - \underline{x}^{(n)}\right) = -f\left(\underline{x}^{(n)}\right) \tag{23}$$

where J is a partial derivative matrix whose component is expressed

$$J \equiv \frac{\partial f_i}{\partial x_i} \quad . \tag{24}$$

By assuming a starting set of $\underline{x}^{(n)}$ values, $\underline{x}^{(n+1)}$ will be calculated based on Equation (23). As has been seen in the preceding section, $\underline{f}$ also requires the information regarding β_1 and β_2 as a function of ξ. Although the body inclinations β_1 and β_2 are specified in the physical plane, we do not know them as a function of mapped potential coordinate ξ until the complete problem is solved. This inherently nonlinear implicit problem is conveniently resolved as a part of the above iterative method by gradually updating β_1 and β_2. The first assumption for β_1 and β_2 is naturally that of constant values, i.e., straight line body assumption. These values are then updated whenever the new set of $\underline{x}$ values are obtained. The iteration procedure will be continued until $\underline{x}$ as well as the functional relations for β_1 and β_2 against ξ converge.

4. PRESSURE DISTRIBUTIONS, FORCE COEFFICIENTS

Once a convergent solution is obtained, the calculations for C_p, C_L and C_D are straightforward.

Since

$$C_p = 1 - \left(q/U_1\right)^2$$

and

$$q^2 = U_2^2 e^{-i(\omega-\omega^*)},$$

thus

$$C_p = 1 - U_2^2 \left[\exp \; I_m \left\{\omega(\xi)\right\} \right]^2 \tag{24}$$

where

$$I_m \left\{\omega(\xi)\right\} = \begin{cases} g_1(\xi) & \text{for } -1 < \xi < b \\ \ell n \sqrt{\frac{1+\sigma}{U_2}} & \text{for } b < \xi < c \\ g_2(\xi) & \text{for } c < \xi < f . \end{cases}$$

The functions $g_1(\xi)$ and $g_2(\xi)$ were already introduced in Equations (14) and (15).

The lift and drag coefficients in the direction of the x- and y- axes are given

$$\overline{C_L} = -\int_{-1}^{f} C_p \; \frac{dx}{ds} \cdot \frac{ds}{d\xi} \cdot d\xi \tag{25}$$

$$\overline{C_D} = \int_{-1}^{f} C_p \; \frac{dy}{ds} \cdot \frac{ds}{d\xi} \cdot d\xi \tag{26}$$

where

$$\frac{dx}{ds} = \begin{cases} \frac{dx}{ds_1} = \cos \beta_1 & \text{for the first arc } S_1 \\ & (-1<\xi<b) \\ \frac{dx}{ds_2} = -\cos \beta_2 & \text{for the second arc } S_2 \\ & (c<\xi<f) \end{cases}$$

$$\frac{dy}{ds} = \begin{cases} \sin \beta_1 & \text{for the first arc } S_1 \\ & (-1<\xi<b) \\ \sin \beta_2 & \text{for the second arc } S_2 \\ & (c<\xi<f) \end{cases}$$

$$\frac{ds}{d\xi} = \begin{cases} \frac{ds_1}{d\xi} = -sg\,(\xi)\,\frac{e^{-g_1(\xi)}}{U_2}\,\frac{dw}{d\xi} & \text{for the first arc } S_1 \\ & (-1<\xi<b) \\ \frac{ds_2}{d\xi} = \frac{e^{-g_2(\xi)}}{U_2}\,\frac{dW}{d\xi} & \text{for the second arc } S_2 \\ & (c<\xi<f) \end{cases}$$

The lift and drag coefficients C_L and C_D in parallel and normal to the incoming flow angle are thus calculated

$$C_L = \overline{C_L} \cos \alpha_1 - \overline{C_D} \sin \alpha_1 \tag{27}$$

$$C_D = \overline{C_L} \sin \alpha_1 + \overline{C_D} \cos \alpha_1. \tag{28}$$

5. RESULTS AND CONCLUSIONS

The present theory was first applied to partially cavitating flat-plate cascades and the results were compared with those of a linearized theory of Wade [13] where the same parameters in [13] are used in Figure 3. Not only the lifting force itself but also the trend of the curves are significantly different between the two theories. The discrepancies particularly become larger as the cavitation number increases. As has been mentioned before, it is considered that these discrepancies are attributable to the loss of the linearized theory's accuracy for larger cavitation number flows. Furthermore, the incidence angle taken in the nonlinear theory, i.e., 8 degrees, may be already beyond the applicable range of the linearized theory.

The theory was also compared with some experimental data of partially cavitating cascade of plano-convex blades [3]. The blade thickness used for the experiment was 8 percent chord. In order to gradually update the present numerical calculations, the thickness of plano-convex blade was changed, starting from 0 percent to 2, 5 and 8 percents. Each computation utilized converged solution of previous results as a starting point of the iterative procedure. The lift and drag coefficients are shown in Figures 4 and 5. Convergent solutions were obtained for 0 and 2 percent thickness cases with the TYPE I B.V.P. in which the cavitation number was specified. The results not only check with the lift coefficients of fully wetted flat plate

cascade calculated based on Thwaites [17], but also show the effects of blade camber as an increase in C_L. The calculated results of 2 percent thickness approach closer to those of the experiment having blades of 8 percent thickness.

We encountered severe numerical instability with the same computer program when the blade thickness was increased to 5 and 8 percents. No matter how carefully initial values were chosen, the length of cavity at each iteration wildly changed over a total range of chord length and never converged. It was this time that the TYPE II B.V.P. approach in which the cavity length is specified and the corresponding cavitation number is determined was used. The problem of numerical instability was resolved with this second method. As was suspected from the occurrence of numerical instability for thickness of 5 percents with the first method, it was found here that the cavity has two different lengths for one cavitation number as shown in Figure 6. The lift and drag coefficients obtained are also plotted in Figures 4 and 5 and showed peculiar behavior in the $C_L - \sigma$ and $C_D - \sigma$ curves. As the cavity length decreases, the cavitation number first increases but then starts decreasing with a slight increase of C_L. It seems that these multiple cavity length solutions and peculiar force-vs.-σ behaviors will well explain the unsteady oscillatory phenomena of the partially cavitating single foil or cascade flows as were observed in experiements [2] and [3]. A recent study of Uhlman and Jiang [15] attributed the existence of two cavity lengths for a specified σ to the inaccuracy of the linearized theory and the inherent flow instability. The first cause is now obviously denied.

The plano-convex foils such as of 0 and 2 percent thickness have a single value of cavity length for a specified σ while as the thickness increases to e.g., 5 percents the cavity length starts having double values. This fact seems to provide an essential key for understanding the above unsteady cavity phenomena. The detailed pressure distributions on the upper blade surface are plotted in Figures 7(a) to (c). For the thickness of 0 and 2 percent cases, it is seen from these figures that the pressure distributions on the upper solid boundary always indicate positive values relative to the cavity pressures C_{pc}. On the other hand, for the blade thickness of 5 percent (Figure 7 (c)), these pressures rapidly become negative relative to C_{pc}, particularly as the cavity length becomes shorter. This violates a theorem applied to the present boundary value problem that the minimum pressure exists inside the cavity (see e.g., a textbook by Birkhoff and Zarantonello [18]) . Furthermore, even taking viscous effects into consideration, high negative pressures cannot be sustained in actual flow field, indicating that the cavity is ready to extend to these lower pressure regions. As soon as the cavity becomes longer, no more low pressure field exists. As is seen in Figure 7 (c), e.g., $\sigma = .37$ case, the vaporization process is not fast enough to provide vapor to hold the cavity. The cavity bubble is thus shed downstream and a new short cavity starts growing.

The generation of higher negative pressures for thicker blades is easily understood; the higher the negative curvature of the obstacle in the flow field, the lower the negative pressure. As a matter of fact, the present explanation for the unsteady partial cavity flow motion based on the steady state flow analysis

is consistent with experimental observations. Experiments of Meijer [2] and Wade and Acosta [3] are two well-known cases in which the unsteady phenomena were observed. Although one tested a single foil and the others cascade foils, a most significant coincidence between the two is that both used blades whose upper profile is of unfavorable shape for the pressure field, i.e., concave shape, in these cases, circular arc. It is now clearly explainable why the unsteady cavity oscillations occurred in both cases.

Based on the above discussions, it is realized that the partially cavitating flow is either stable or unstable, depending upon the pressure distributions on the wetted part of the upper blade surface. Figure 6 indicates the stable partial cavity condition for thin flat-plate cascades. In the past, little hydrodynamic considerations have been given for design of blade backside profile. For example, the backside profiles of supercavitating propellers were determined from a structural integrity point of view within the limit of cavity envelope. In order to avoid the occurrence of cavity oscillations if such propellers operate at an off-design point in the partially cavitating regime, it is recommended that the blade backside profile be properly designed so that favorable pressure distributions Cp prevail. At least, Cp on the backside of blades under several partially cavitating conditions must be investigated during the design procedure; it should be ensured that C_p is much larger than $-\sigma$ over the full range of wetted upper boundary.

Unlike linearized partial cavity or super cavitating theories, the present nonlinear partial cavity theory has no singular behaviors as ℓ_c approaches the chord length nor does the nonlinear super-cavity theory [14]. In Figures 4 and 5, the regimes as ℓ_c becomes c are depicted by dashed lines. This does not mean that C_L and C_D are unknown or become infinite, but they simply have slight discrepancies between the two nonlinear theories because the flow models used for the partial and super-cavity regions cannot be smoothly blended.

Figure 8 shows the boundary profiles of typical partial cavities for $\alpha_1 = 9°$, $\gamma = 36°$ and blade thickness of 2 percents at various cavitation numbers or cavity lengths.

Finally, it must be noted that the numerical iterative method used here provided stable convergent solutions as long as one chose a right type of input data set-up as has been mentioned above. Computer execution time, however, was found to be two to six times that of supercavitating cascade computations in [14].

6. REFERENCES

[1] Knapp, Daily and Hammit, CAVITATION, McGraw Hill Book Company, New York, 1970.

[2] Meijer, M.C., "Some Experiments on Partly Cavitating Hydrofoils", International Shipbuilding Progress, Vol. 6, No. 60, August 1959.

[3] Wade, R.B., and Acosta, A.J.,"Investigation of Cavitating Cascade", ASME, Journal of Basic Engineering, December 1967, 693-706.

[4] Søndvedt, T. and Frivold, H., "Low Frequency Variation of the Surface Shape of Tip Region Cavitation on Marine Propeller Blades and Corresponding Disturbances on Nearby Solid Boundaries", Eleventh Symposium of Naval Hydrodynamics, Sponsored by the Office of Naval Research, University College London, 28 March-2 April 1976.

[5] Bohn, J.C., "Model Tests of a Supercavitating Propeller Designed for a Hydrofoil Ship", Hydronautics Technical Report, 7607.59, August 1977.

[6] Peck, J.G., "Cavitation Performance Characteristics of Supercavitating Propellers 4698 and 4699", David W. Taylor Naval Ship Research and Development Center of the U.S. Navy, Ship Performance Department Report SPD-680-02, December 1977.

[7] Acosta, A.J., "An Experimental Study of Cavitating Inducers", Second Symposium on Naval Hydrodynamics of Office of Naval Research, August 25-29, 1958, Washington, D.C., 533-557.

[8] Acosta, A.J., "A Note on Partial Cavitation of Flat Plate Hydrofoils", Hydrodynamics Lab., California Institute of Technology, Report No. E-19.9, 1955.

[9] Geurst, J.A., "Linearized Theory for Partially Cavitated Hydrofoils", International Shipbuilding Progress, Vol. 6, No. 60, August 1959.

[10] Geurst, J.A., and Verbrugh, P.J., "A Note on Camber Effects of a Partially Cavitated Hydrofoil", International Shipbuilding Progress, Vol. 6, No. 61, September 1959.

[11] Wade, R.B., "Linearized Theory of a Partially Cavitating Plano-Convex Hydrofoil Including the Effects of Camber and Thickness", Journal of Ship Research, Vol. 11, No. 1, March 1967.

[12] Golden, D.W., "A Numerical Method for Two-Dimensional, Cavitating, Lifting Flow", Report No. 81512-1, Department of Ocean Engineering, M.I.T., May 1975.

[13] Wade, R.B., "Flow Past a Partially Cavitating Cascade of Flat Plate Hydrofoils", Division of Engineering and Applied Science, California Institute of Technology, Report No. E79-4, January 1963.

[14] Furuya, O., "Exact Supercavitating Cascade Theory", ASME, Journal of Fluids Engineering, Vol. 97, December 1975, 419-429.

[15] Uhlman, J.S., Jr., and Jiang, C.W., "Experiments on a Partially Cavitating Plano-Convex Hydrofoil with Comparison to Theory", M.I.T. Report No. 83481-2, July 1977.

[16] Tulin, M.P., "Supercavitating Flows -- Small Perturbation Theory", Journal of Ship Research, Vol. 13, No. 3, 1964, 16-37.

[17] Thwaites, B., INCOMPRESSIBLE AERODYNAMICS, Oxford at the Clarendon Press, 1960, 532.

[18] Birkhoff, G. and E.M. Zarantonello, JETS, WAKES, AND CAVITIES, Academic Press, Inc., New York 1957.

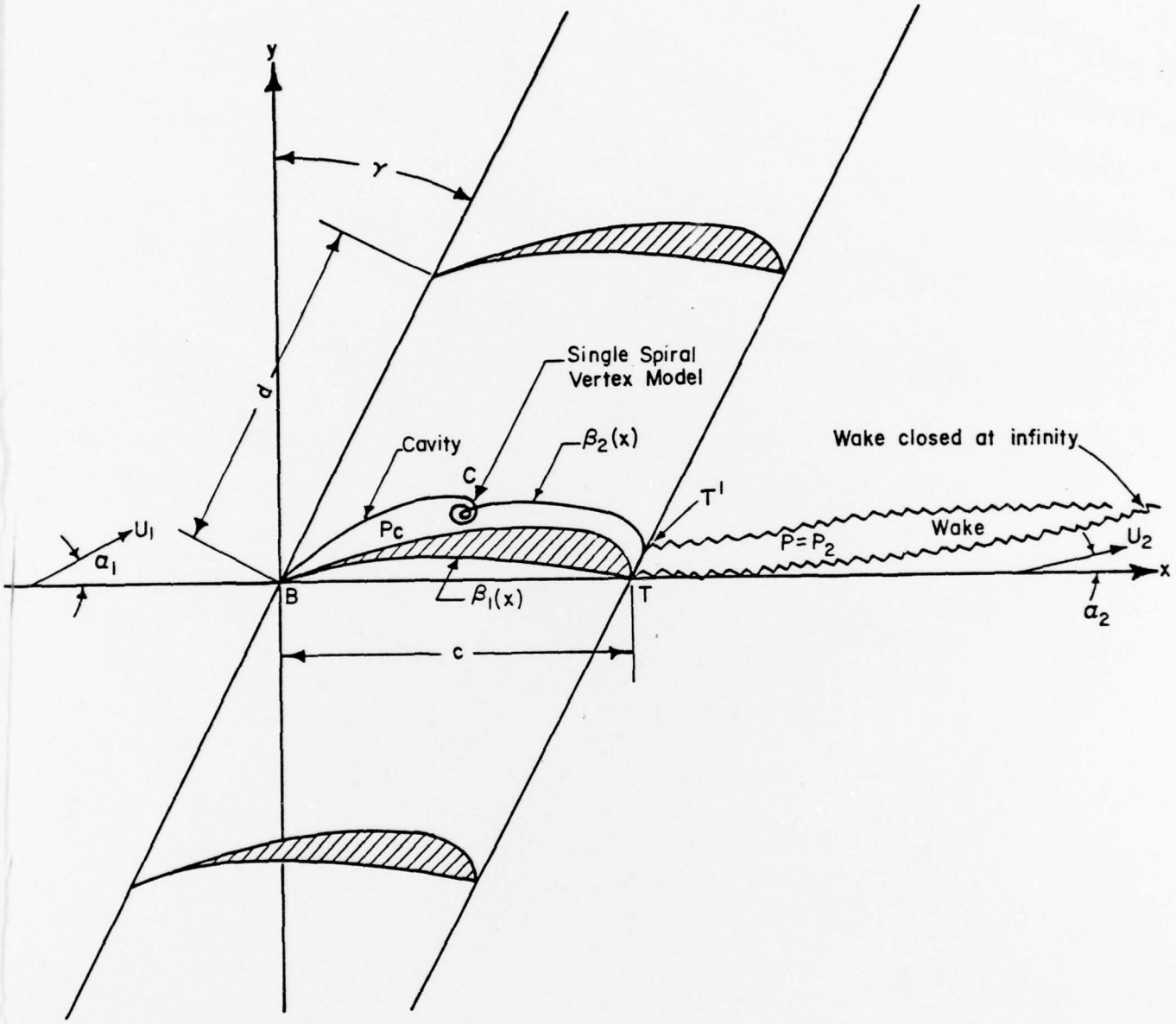

Figure 1 Flow configuration for partially cavitating cascade

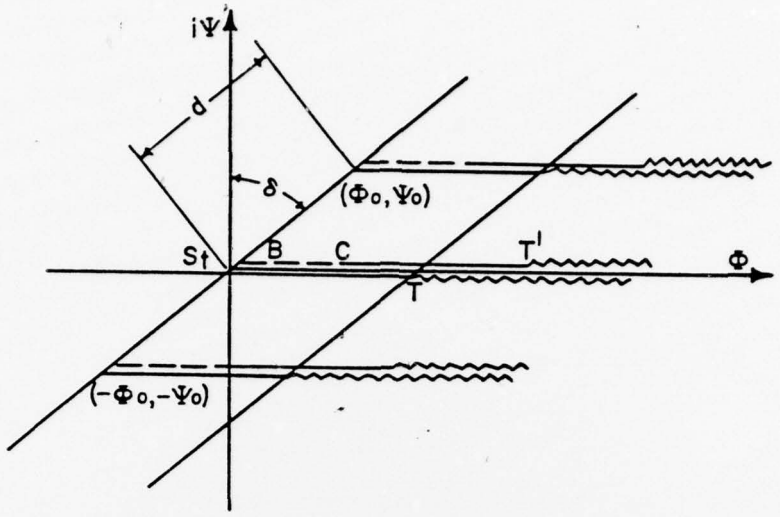

(a) Potential plane $W = \Phi+i\Psi$

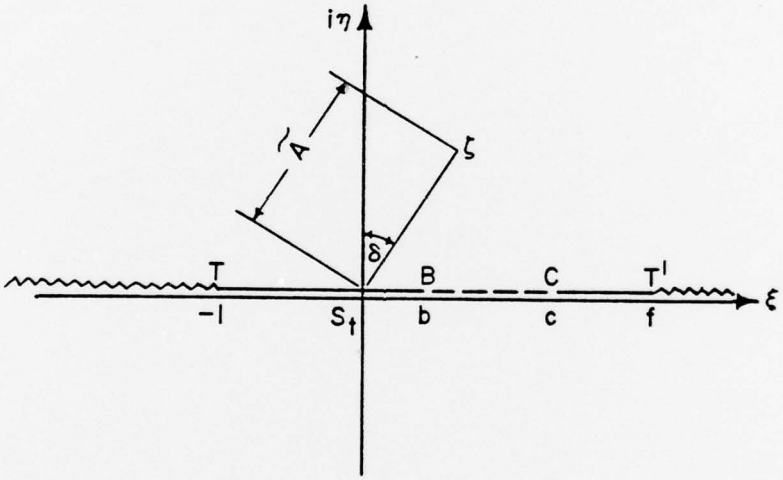

(b) Transform plane $\zeta = \xi+i\eta$

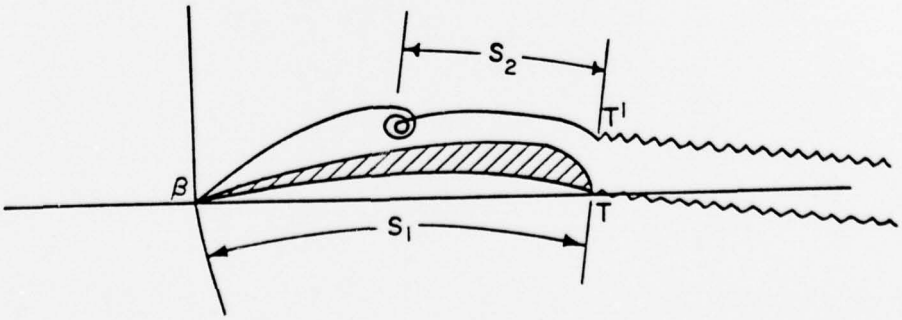

(c) Definition of arc lengths S_1 and S_2.

Figure 2 Two transform planes and definition of arc lengths S_1 and S_2.

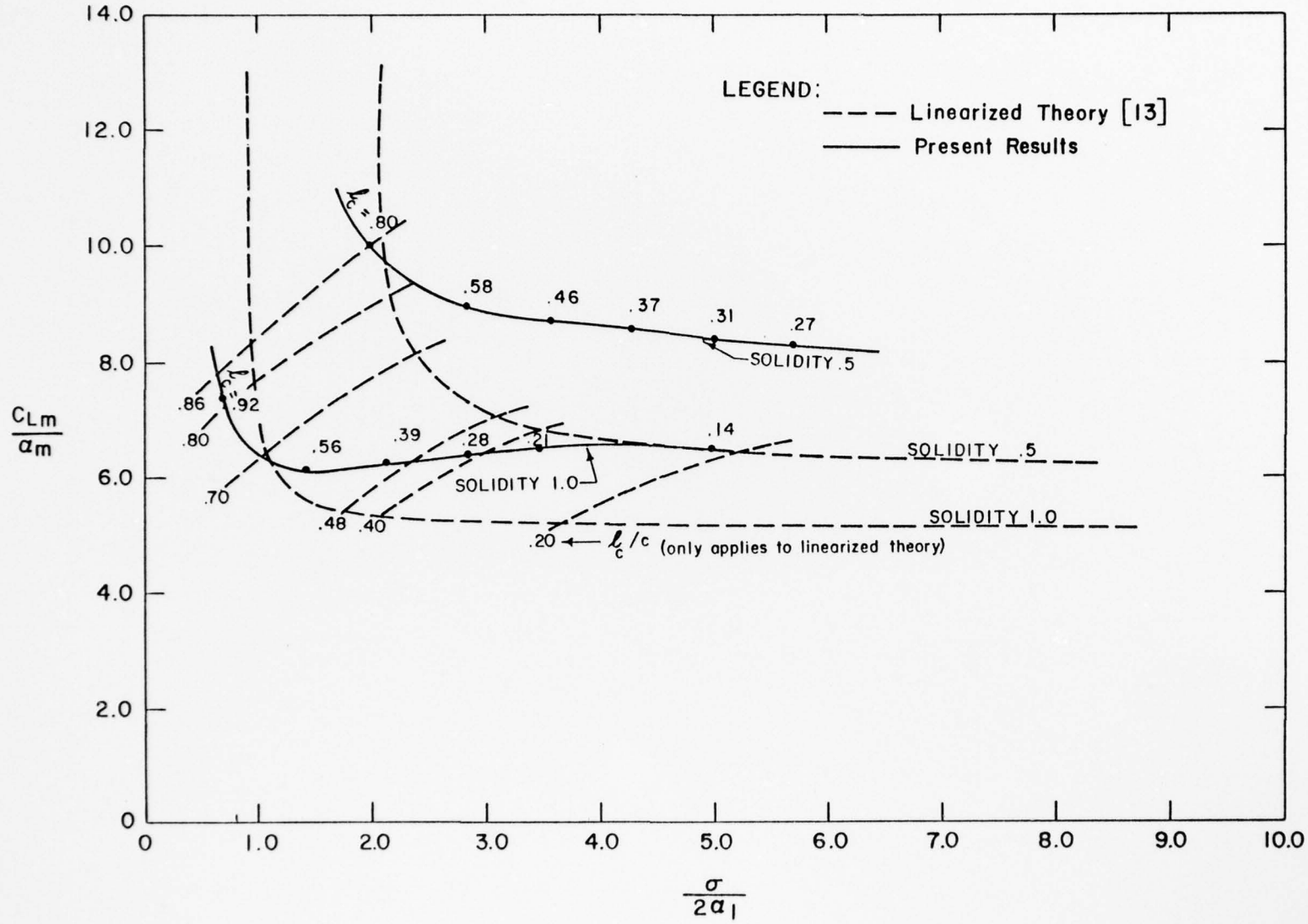

Figure 3 Comparison of the present theory with a linearized theory of Wade [13] for flat-plate cascade at $\alpha_1 = 8°$, $\gamma = 45°$ for two solidity cases, .5 and 1.0.

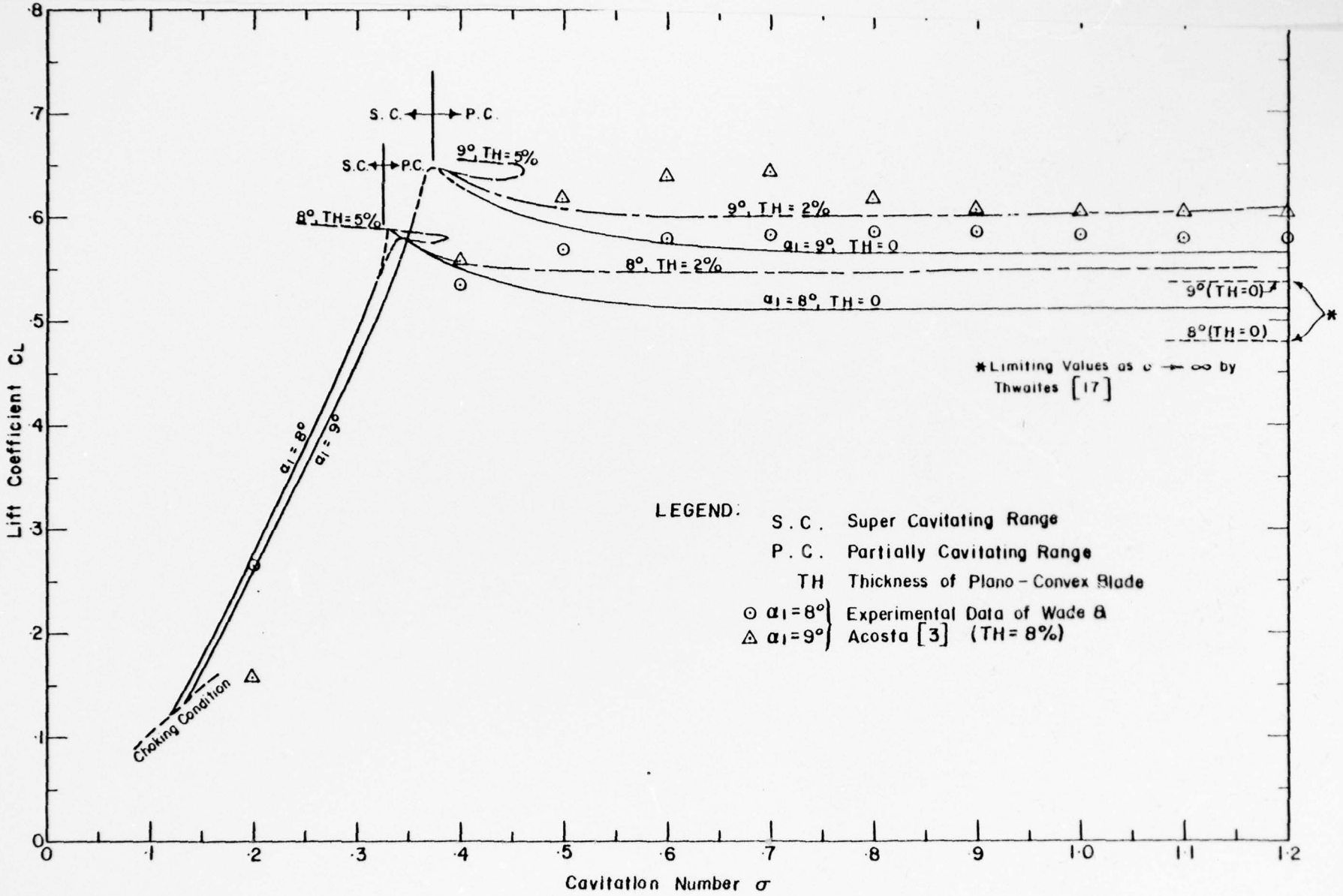

Figure 4 Comparison between the theory and experiment for plano-convex cascade having various blade thickness where solidity is .625 and stagger angles are 37° and 36° for α_1 = 8° and 9°, respectively (calculated data for supercavitating range made with [14] are also included).

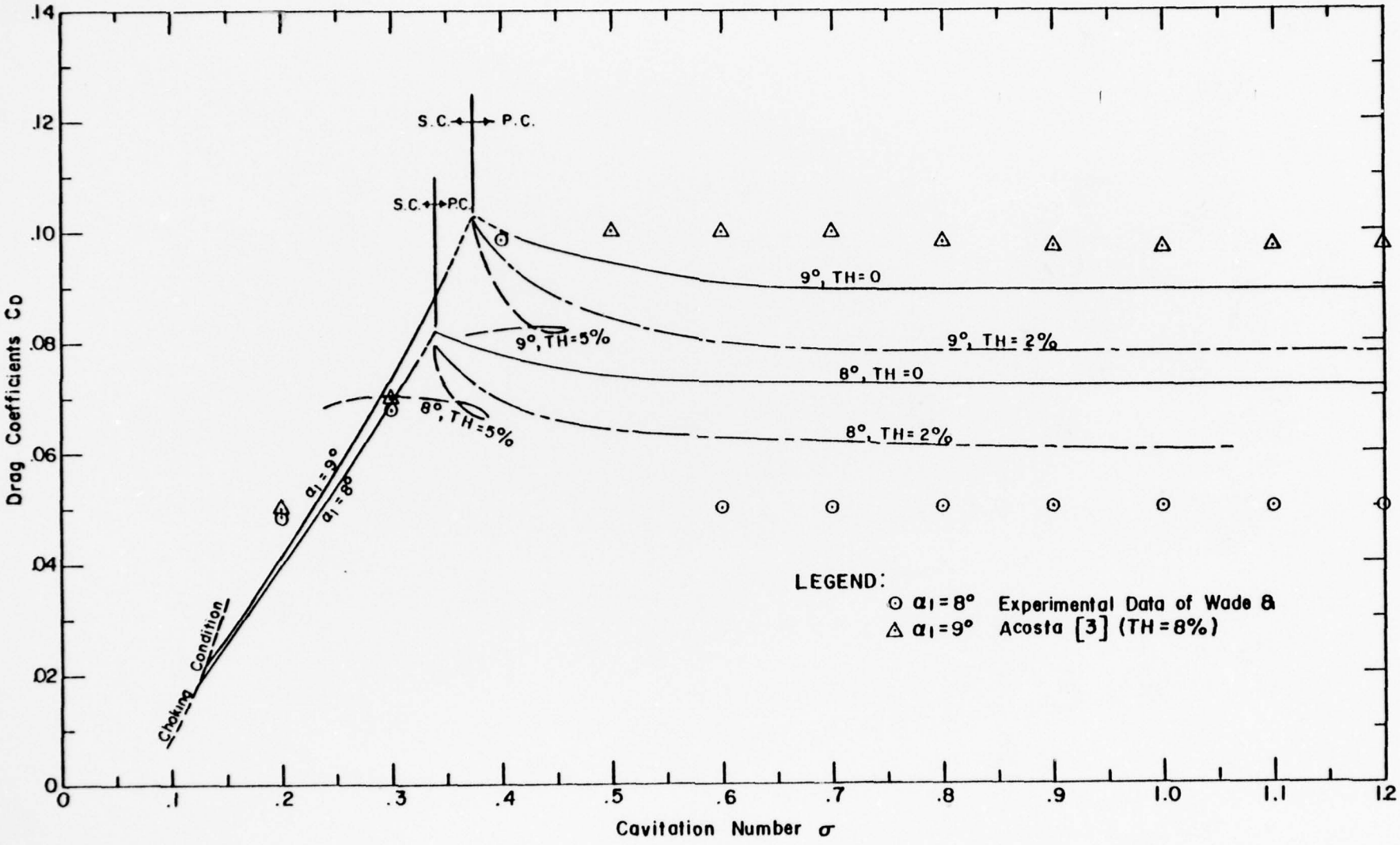

Figure 5 Drag coefficients for the same cases as Figure 4

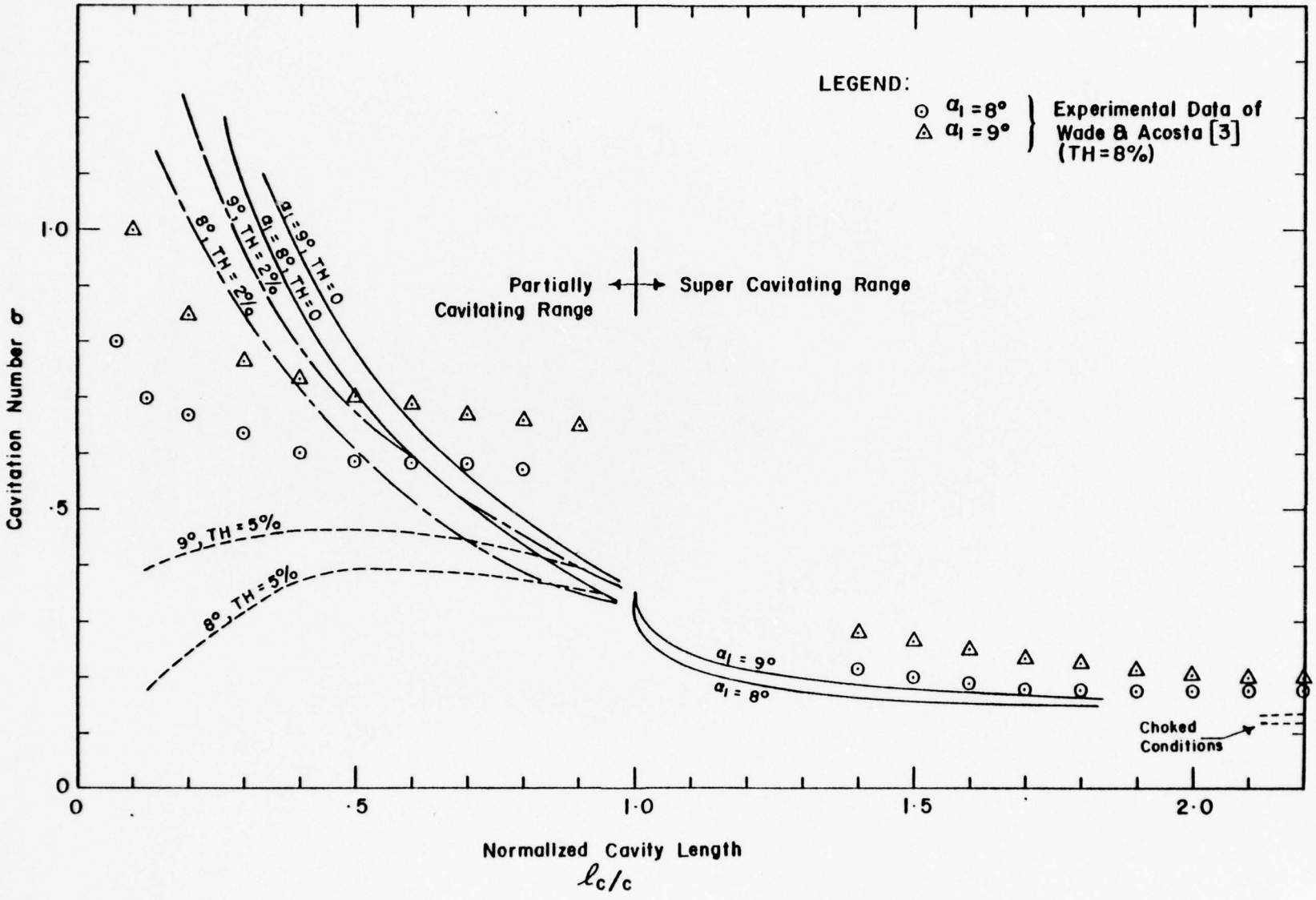

Figure 6 Cavity length vs. cavitation number for the same cases as Figure 4.

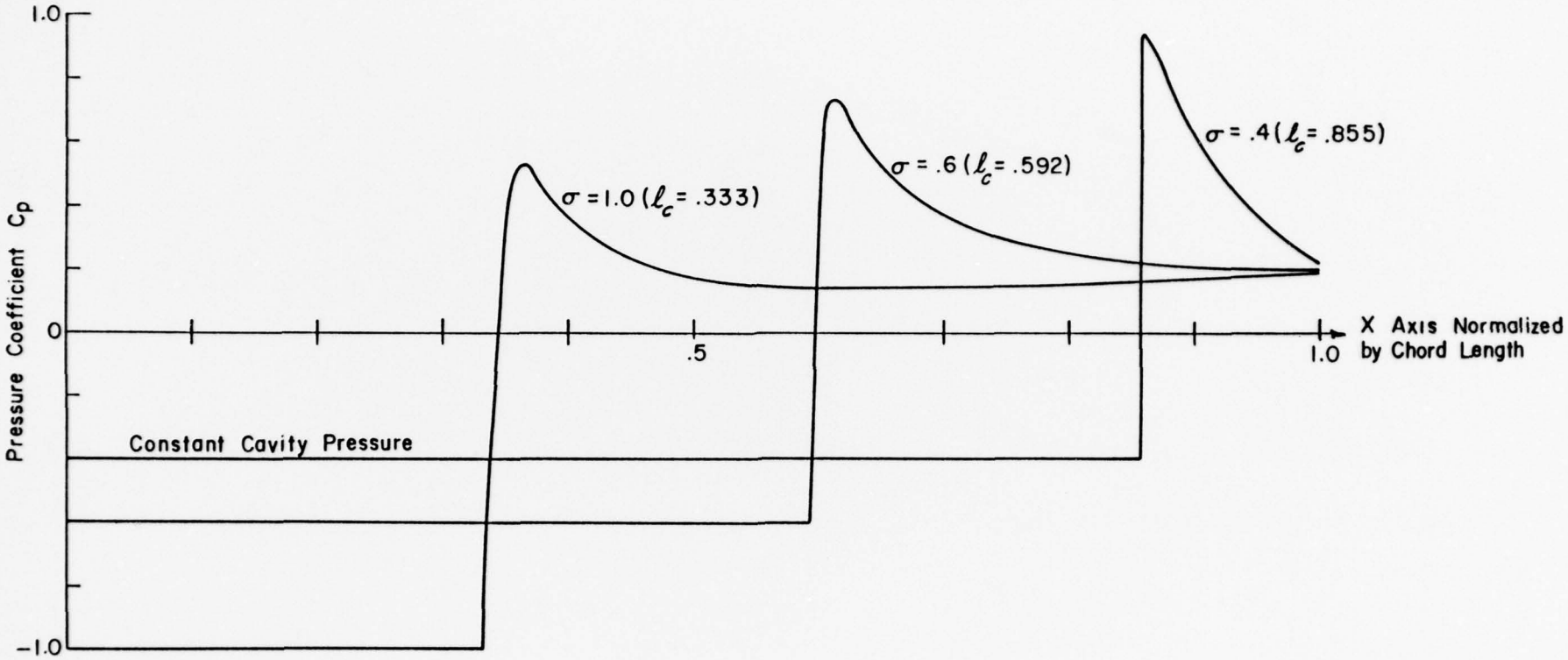

Figure 7(a) Calculated pressure distribution on the upper wetted portion of plano-convex blade of partially cavitating cascade having 0 percent thickness for various cavitation numbers.

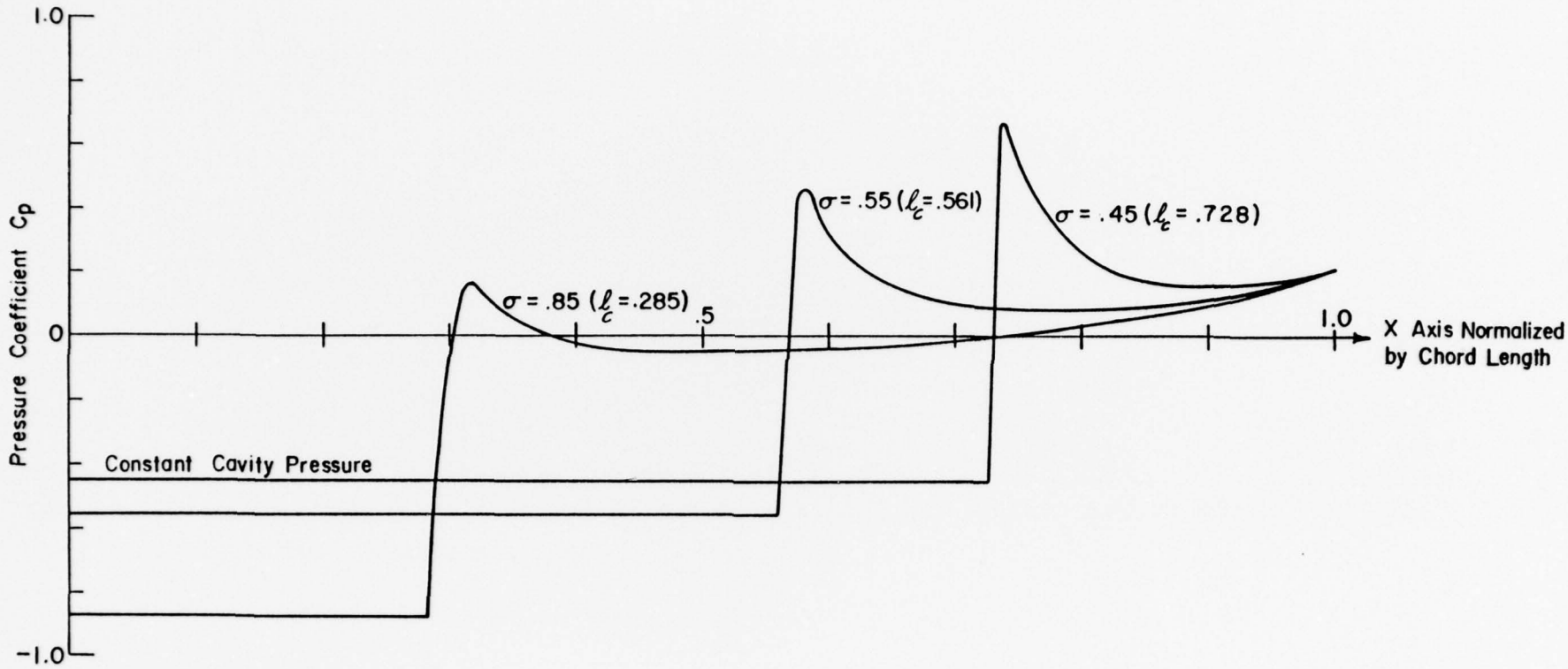

Figure 7(b) The same as Figure 7(a) except for TH = 2%.

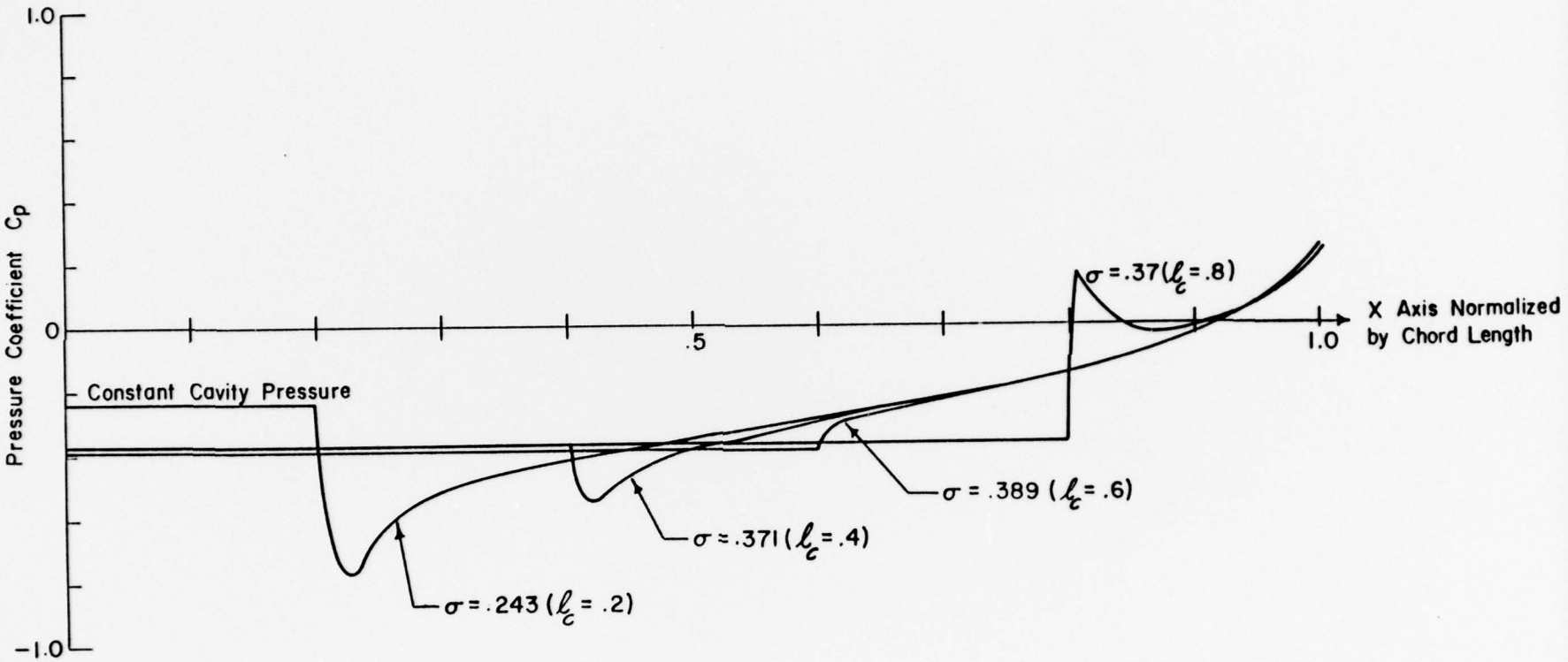

Figure 7(c) The same as Figure 7(a) except for TH = 5%.

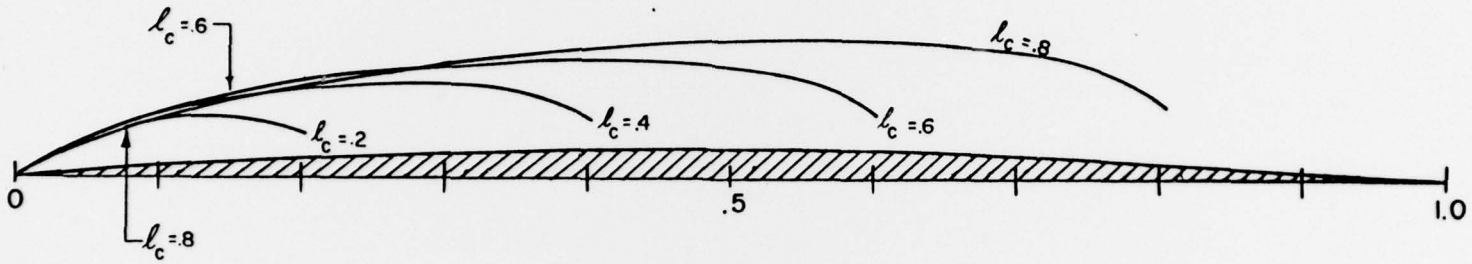

Figure 8 Profiles of calculated cavity boundaries for cascade of plano-convex blades having 2% thickness at α_1=9° with γ=36° and solidity = .625